Global Curve Analysis via a Dimensionality Lifting Scheme

Gershon Elber
Computer Science Department
Technion
Haifa 32000, Israel
Email: gershon@cs.technion.ac.il

Technion, Israel Institute of Technology,
Haifa 32000, Israel
gershon@cs.technion.ac.il

Abstract. Freeform rational parametric curves and surfaces have been playing a major role in computer aided design for several decades. The ability to analyze local (differential) properties of parametric curves is well established and extensively exploited. In this work, we explore a different lifting approach to global analysis of freeform geometry, mostly curves, in $\mathbb{R}^2$ and $\mathbb{R}^3$. In this lifting scheme, we promote the problem into a higher dimension, where we find that in the higher dimension, the solution is simplified.

1 Introduction

The differential analysis of freeform planar and 3-space parametric curves is a fundamental tool that is heavily used in computer aided geometric design applications. Numerous examples exist. Being able to handle and define curvature properties eases the understanding of singularities in offset curves, curves that are crucial to many design and manufacturing applications. Having the ability to locally define a wide variety of orientation frames along curves, from the Frenet [6] frame to orientation minimizing frames [4, 17] using local differential geometry, constitutes an immense aid in the construction of sweep surfaces.

The exploited differential analysis is indeed mostly local. Analysis of the global properties of curves (and surfaces) in $\mathbb{R}^2$ and $\mathbb{R}^3$ is far less common in geometric design. Clearly, global integrable properties of freeform geometry are much more difficult to detect. Some examples of work that has tried to derive global properties are found in [14] where moments of freeform geometry are developed. In [9, 15, 18], the area (volume) enclosed by a curve (surface) is made fixed while interactive (multi-resolution) direct manipulation is allowed. In the present work, we consider a different approach to global analysis of freeform geometry. By lifting the problem into a higher dimensional space, the hope is that the lifted geometry will, in fact, be simpler to process.

We intend to explore several problems about which very little is known. Yet and as an example, we take as our starting point the simple and already solved problem of finding all the inflection points of a freeform regular planar curve, $C(u)$. This problem is closely related to the issue at hand and could easily be reduced to finding the zeros of the univariate of $C''(u) \times C'(u)$, thereby identifying all the locations with zero curvature in the curve. Nonetheless, in Section 2, we will use this example to show a new constructor – an *orthogonality map* – that lifts the univariate curve $C(u)$ into a bivariate surface. With this map, the identification of all the inflection points is simple. Further, other (global) properties of planar curves such as visibility properties and their winding numbers will also be revealed with the aid of the orthogonality map.

Visibility and moldability are two other examples where global analysis must play a role. Visibility queries typically ask questions regarding lines-of-sight between points and objects whereas the moldability question looks at partitioning the given geometry into parts of a mold that can be assembled and disassembled without the parts colliding. Interestingly enough, these two problems are closely related. Consider the planar n-moldability problem of $C(u)$. That is, the computation of the decomposition of $C(u)$ into an n-piece mold, if possible, minimizing n. While some work on piecewise linear representations (i.e., polygons) can be found, virtually nothing is known about this problem and its solutions in the context of freeform geometry. In [1], the two-piece mold separability problem for polygonal surfaces in $\mathbb{R}^3$ is considered, with a heuristic implemented solution. View and inspection planning is another problem that was investigated in this piecewise linear context [19].

In the freeform domain, little information exists about visibility and moldability. A previous paper by Elber [12] considered the problem of determining the existence of a valid two-piece mold for a designed solid model whose boundary is represented as a NURBS surface with C^3 continuity, and finding such a mold if it exists. For more than two pieces, nothing is known. Moreover, related visibility problems such as the art gallery query, a well studied problem in the computational geometry community, again in the discrete polygonal domain [3], is another open question. In Section 3, we will address these questions using a different dimensionality lifting scheme.

Another problem we will be exploring in Section 4 is, given a simple 3-space curve, $C(u)$, find all directions V, if any, in $\mathbb{R}^3$ from which $C(u)$'s orthographic projection onto the plane orthogonal to V is simple. Finally, in Section 5, we conclude.

2 The Orthogonality Map

Consider a C^1 regular planar parametric curve $C(u)$:

Definition 1. *The* Orthogonality Function $\mathcal{O}_{\mathcal{F}}(u, v)$ *of a* C^1 *regular planar parametric curve* $C(u) : \mathcal{D} \in \mathbb{R} \rightarrow \mathbb{R}^2$ *is defined as*

$$\mathcal{O}_{\mathcal{F}}(u, v) = \langle C'(u), C'(v) \rangle : [\mathcal{D} \times \mathcal{D}] \rightarrow \mathbb{R}.$$

and

Definition 2. *The* Orthogonality Map $\mathcal{O}_{\mathcal{M}}$ *of a* C^1 *regular planar parametric curve* $C(u)$*, denoted* $\mathcal{O}_{\mathcal{M}}[C]$*, is the zero set of the orthogonality function,* $\mathcal{O}_{\mathcal{F}}(u,v)=0$*.*

The orthogonality function lifts curve $C(u)$ into an explicit surface whose zero set is defined to be the curve's orthogonality map. Let us explore a few properties of the orthogonality map.

Lemma 1. $\mathcal{O}_{\mathcal{F}}(u,v)$ *and* $\mathcal{O}_{\mathcal{M}}[C]$ *are both symmetric along the* $u=v$ *diagonal for a closed* C^1 *curve* C*.*

Proof. Trivial by construction, $\mathcal{O}_{\mathcal{M}}(u,v)=\mathcal{O}_{\mathcal{M}}(v,u)$.
■

The fact that the $\mathcal{O}_{\mathcal{M}}$ map is symmetric will repeat itself in the other lifting schemes we will examine. Since $\mathcal{O}_{\mathcal{F}}(u,v)$ is a continuous function, all curves in $\mathcal{O}_{\mathcal{M}}[C]$ are either closed loops or curves that start and end on the boundary of $[\mathcal{D}\times\mathcal{D}]$.

Recall that we sought, as a simple exemplary motivation, to derive all the inflection points of the planar curve $C(u)$ using $\mathcal{O}_{\mathcal{M}}$. The following result explains how this could be accomplished:

Lemma 2. *The* u*-extreme (*v*-extreme) locations in* $\mathcal{O}_{\mathcal{M}}[C]$ *correspond to* v*-inflection (*u*-inflection) points in* C*.*

Proof. The extreme locations of the subset of $\mathbb{R}^2$ of $\mathcal{O}_{\mathcal{F}}(u,v)=0$ (the $\mathcal{O}_{\mathcal{M}}$ set) are classified by the additional constraints of $\frac{\partial\mathcal{O}_{\mathcal{F}}(u,v)}{\partial v}=0$ $\left(\frac{\partial\mathcal{O}_{\mathcal{F}}(u,v)}{\partial u}=0\right)$ [16]. These are the locations where the $\mathcal{O}_{\mathcal{M}}$ curve has u-extreme (v-extreme) locations.

Differentiating $\mathcal{O}_{\mathcal{M}}(u,v)$ with respect to u (respectively v),

$$\frac{\partial\mathcal{O}_{\mathcal{F}}(u,v)}{\partial u}=\frac{\partial\left\langle C'(u),C'(v)\right\rangle}{\partial u}=\left\langle C''(u),C'(v)\right\rangle=C''(u)\times C'(u),$$

due to the fact that $C'(v)$ is orthogonal to $C'(u)$, satisfying $\mathcal{O}_{\mathcal{F}}(u,v)=0$ (similarly for the case of v).

Nevertheless, the condition $C''(u)\times C'(u)=0$ is exactly related to the zero curvature locations, hence detecting the inflection points.
■

Figure 1 presents an example of a planar curve (Figure 1 (a)) and its orthogonality map (Figure 1 (b)). In Figure 1 (c), the orthogonality function is shown in $\mathbb{R}^3$ along with its zero set, the orthogonality map. Two inflection points are presented in Figure 1 (a) and these points are clearly reflected as extreme locations in the orthogonality map shown in Figure 1 (b). Note the two pairs of lines (one horizontal pair and one vertical pair) in Figure 1 (b) at the inflection points' parameter values go through all the extreme locations, capturing the loops in the map as well.

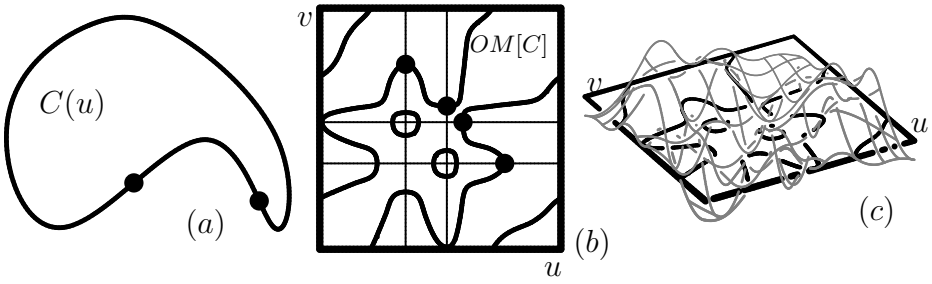

Fig. 1. An orthogonality map $OM[C]$ (b) of a planar curve $C(u)$ (a). (c) presents the orthogonality function (in gray) along with its zero set (in black), the orthogonality map.

Definition 3. *Consider a sub-region of* $C(v)$, $v_1 < v < v_2$. $C(v)$, $v_1 < v < v_2$ *is considered* locally visible *from some view direction* V, *if no point* $C(v_0)$, $v_1 < v_0 < v_2$ *obscures another point in that domain, when viewed from* V.

Put differently, the local visibility only considers the possibility of a small region of $C(u)$ to obscure itself, and ignores the possibility that other parts of $C(u)$, outside the local domain, obscure these points. Consider now the viewing direction of $V = N(u_0)$, following the normal of C at u_0. Inspect the point (u_0, u_0) on the diagonal of $\mathcal{O}_{\mathcal{M}}[C]$ and shoot two opposing rays vertically, in the $-v$ and $+v$ directions, from (u_0, u_0) (see the vertical light-gray edge in Figure 2 (c)). Let the points of impact of these vertical rays with $\mathcal{O}_{\mathcal{M}}[C]$ be (u_0, v_1) and (u_0, v_2) and denote these points as the *vertically closest* points to (u_0, u_0).

Lemma 3. *Let* (u_0, v_1) *and* (u_0, v_2) *be the two vertically closest points on* $\mathcal{O}_{\mathcal{M}}[C]$ *to* (u_0, u_0), *for some* u_0. *Then, the region of* C *from* $C(v_1)$ *to* $C(v_2)$ *is locally visible from direction* $V = N(u_0)$.

Proof. By the orthogonality map, every point $C(v)$, $v_1 < v < v_2$ possesses a tangent vector that is never orthogonal to $C'(u_0)$ and hence is never parallel to V. Consequently, starting from $C(u_0)$, when we move along the curve toward $C(v_1)$ (or toward $C(v_2)$), we never locally occlude previous curve points in the domain. In other words, none of the curve points $C(v)$, $v_1 < v < v_2$, could possibly occlude each other and, therefore, they are all locally visible.
■

Figure 2 is an example of this phenomenon. In Figure 2 (a), a planar curve is presented with the point $C(u_0)$ for which the local visibility is sought when viewed from $N(u_0)$ (see Figure 2 (d)). With the aid of the orthogonality map in Figure 2 (b), the local visibility of $C(u_0)$ could be determined, as shown in Figure 2 (c) in light-gray.

One can build the lower, $L(u)$, and upper, $U(u)$, envelope of these local visibilities for all u locations in the domain of $C(u)$. These envelopes show, for all u, the maximal extent along the curve that is locally visible from $N(u)$ – the normal direction at $C(u)$. These lower and upper envelopes of the local visibility,

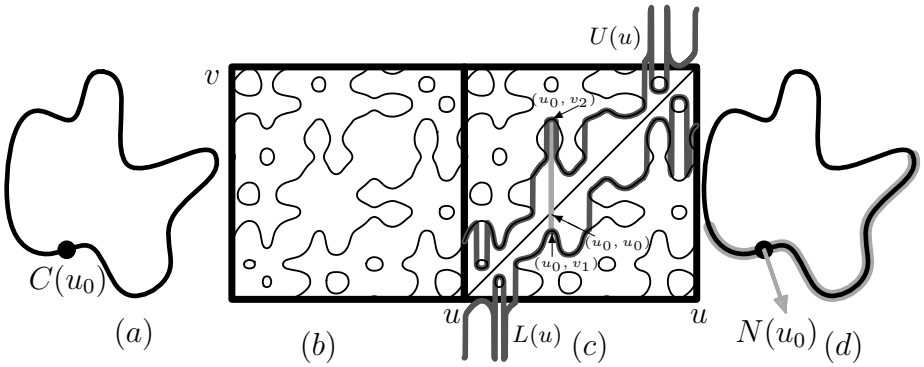

Fig. 2. The orthogonality map (b) of planar curve (a) is used to compute the local visibility (light-gray in (c) & (d)) from direction $N(u_0)$. Over all u, the lower, $L(u)$, and upper, $U(u)$, visibility envelopes are constructed and shown in (c) in dark-gray.

as was determined for all u in the domain, are plotted in Figure 2 (c), in dark-gray. If the geometry is closed and C^1 continuous, the map is periodic in both the u and v axes and hence the envelopes penetrate above (below) the square domain with the semantics that these portions are warped to the bottom (top) of the domain.

$L(u)$ and $U(u)$ could aid in selecting a minimal set of views from which the entire curve is (locally) accessible or visible. More on this will be found in Section 3.

The orthogonality map comprises two types of entities. The first are islands that are the result of having two inflection points in the curve with tangents that are (almost) orthogonal. In Figure 1 (b), we have one such island (note we consider only one half of this symmetric function). This island corresponds to the two inflection locations marked on Figure 1 (a).

The second type of entity is composed of components that start at the bottom boundary and end at the right boundary (considering only the portion of the orthogonality map below the diagonal). Note that both islands could cross boundaries if the curve is periodic, and components that start at the bottom boundary and end at the right boundary could also traverse back and forth across these boundaries. Now, consider this periodic map, for periodic curves, as a repeated square that tiles $\mathbb{R}^2$, while denoting the original map as the *primary tile* (see Figure 3).

Let $\mathcal{W}$ denote the *winding number* of curve $C(u)$, i.e., the number of times the curve turns in the plane. $\mathcal{W}$ could be computed by integrating the curvature of the curve, yet we postulate that this global number could also be extracted from the orthogonality map. Count the number of paths from the bottom boundary through the right boundary. Then, we have the following result:

Observation 1 *The number of infinite paths from the bottom boundary to the right boundary of the orthogonality map equals* $2\mathcal{W}$.

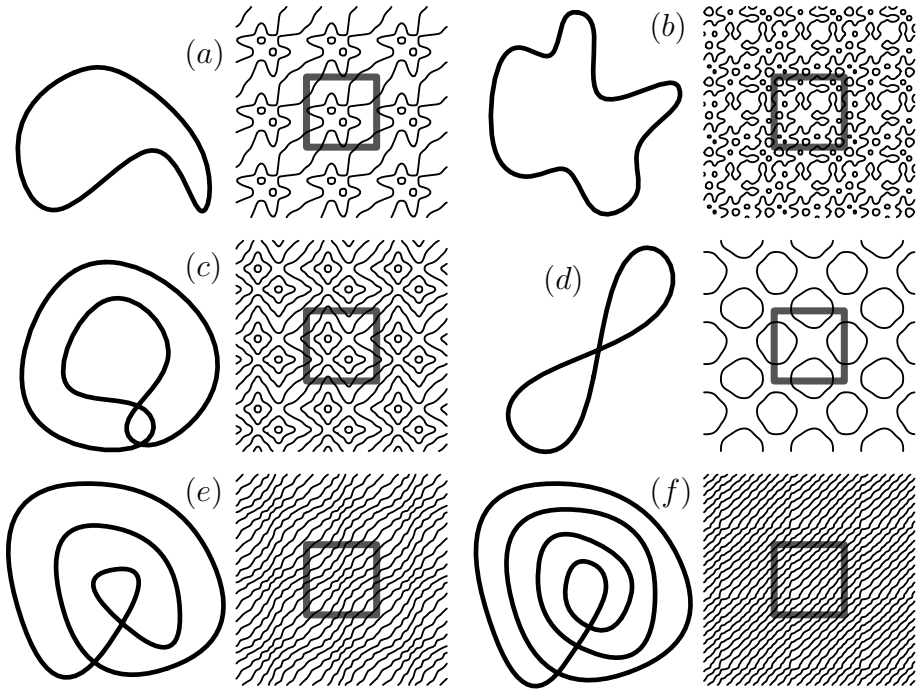

Fig. 3. The winding number of a planar curve is equal to half the number of infinite paths going through the bottom boundary to the right boundary of the primary tile (in gray) of the orthogonality map.

To justify this observation, consider $C(u)$ to be a closed, simple, continuous convex curve (see Figure 4 (a) and consider an infinite line in the direction of $D = C'(u_0)$ approaching from infinity in the $N(u_0)$ direction and toward $C(u)$, $N(u_0)$ being the normal of C at u. Stop the approach at the first point of contact with $C(u)$, and repeat this line-approaching process from the $-N(u_0)$ direction. The distance between these two infinite parallel lines, which are now in contact with $C(u)$ on both its sides, determines the diameter of the convex curve from that direction (which cannot be zero). Hence, a simple closed convex curve has a pair of solution points on the orthogonality map, for every location on the curve. $C(u)$ is C^1 continuous and due to this continuity these pairs will combine and form two continuous paths on the orthogonality map from the bottom boundary to the right boundary. For a convex curve, these paths will also be monotone.

The convex hull curve of every planar simple curve will, therefore, have two paths. The convex hull of a planar simple curve $C(u)$ consists of convex regions of $C(u)$ and line segments connecting these regions (see Figure 4 (b)). Nonetheless, the line segments are bitangent lines to $C(u)$ that have the same tangent direction at the two end points of each line segment, denoted $C(u_s)$ and $C(u_e)$. A path in the orthogonal map that matches another point $C(u_m)$ as an orthogonal

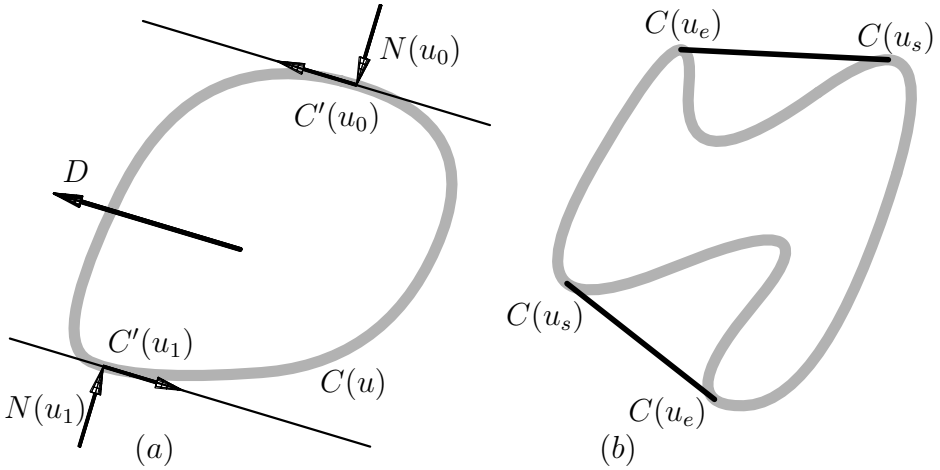

Fig. 4. Given some direction $D = C'(u_0)$ in (a), two inifinite lines in direction D approach convex planar curve $C(u)$ from $\pm N(u_0) = \mp N(u_1)$ and touch it in two locations u_0 and u_1. In (b), a general curve is complemented with bitangents, making it convex.

point to $C(u_s)$ must be connected to $C(u_e)$ as well, because the curve segment $C(u)$, $u \in [u_s, u_e]$ is C^1. In other words, the two paths will still form, for a simple curve, though they will no longer be monotone.

Now consider m nested, closed, simple C^1 continuous convex curves. Clearly, every such simple curve contributes two paths or $2m$ paths in the orthogonality map in all. Nevertheless, every closed curve could be broken into several closed and simple curves, while preserving the orientation of the loops to follow that of the original curve. For example, Figure 5 shows a decomposition of the curve in Figure 3 (f) into four simple and nested curves.

The two curves in Figures 3 (a) and (b) are simple and the primary tile indeed has two paths from the bottom boundary to the right boundary. The self intersecting shape in Figure 3 (c) is decomposed into three simple loops, but one of them is in the opposite orientation to the other two and hence the two paths from the bottom boundary to the right boundary of the primary tile prescribe the correct winding number. The self intersecting '8' shape in Figure 3 (d) is decomposed into two simple curves but in an opposite orientation, which leaves the winding number of this curve at zero. Finally, the two shapes in Figures 3 (e) and (f) are decomposed into three and four simple nested curves, all with the same orientation and as expected, six and eight paths are recognized in their primary tiles, respectively.

Given an orthogonality map, one needs to trace all the closed loops in the map and purge them away so as to find and count only the continuous paths that originate at the bottom boundary and end at the right one. This tracing process is trivial as loops are detected by tracing until one ends up at the starting location. The other tracing alternative is to start at the right boundary and

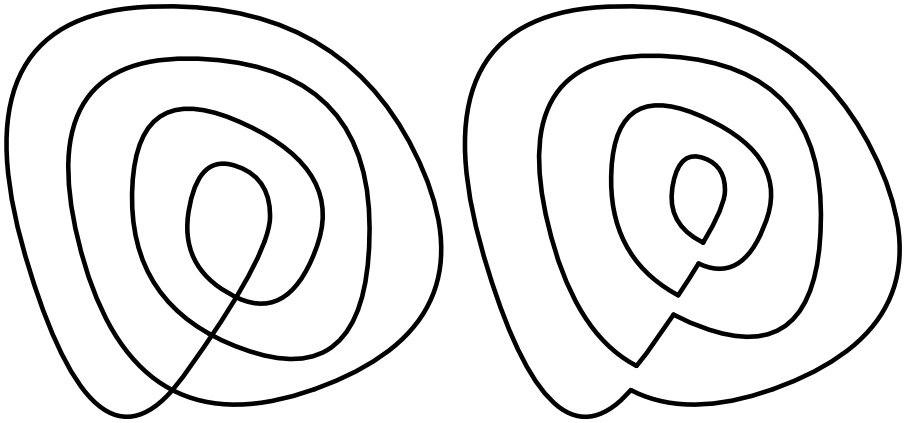

Fig. 5. A decomposition of a curve with four loops (a) into four simple nested curves (b). See also Figure 3 (f).

then the curve, if not a loop, must end up at the bottom boundary. In recent years, the recovery of the topology of implicit forms, as is $\mathcal{O}_{\mathcal{M}}[C]$, has also been investigated. These recovery methods, for example [16], could be used to recover the winding number of $C(u)$ without explicitly tracing the entire orthogonality map.

3 The Visibility Question

Going beyond the orthogonality maps, we would like to consider global visibility as well. This means that, for every point of inspection, one needs to resolve the (view) point-curve visibility problem. The visibility could change at the silhouette curves' locations, $\mathcal{S}$ – locations where the view direction V is tangent to the curve $C(u)$ or $\mathcal{S} = \{u \mid \langle V, N(u)\rangle = 0\}$, where $N(u)$ is the normal field of C. We seek to split $C(u)$ at all locations where the quantitative invisibility [2, 7] changes. The original quantitative invisibility [2] algorithm starts by splitting all polygonal edges with inhomogeneous visibility in the projection plane into homogeneous segments. That is, if a polygonal edge is partially visible and partially hidden, it is split at the location where the visibility changes. [7] extended this work to freeform surfaces.

Reflecting on the problem at hand and seeking curve segments with homogeneous visibility from V, we need to split planar curve $C(u)$ at its silhouette points, $\mathcal{S}$. However, we also need to split $C(u)$ at all locations along the line of sight from V through $u \in \mathcal{S}$ that pierce C after the silhouette locations. These are the curve locations that become (in)visible behind silhouette points when viewed from V. Figure 6 shows an example. In (a), the silhouette locations of $C(u)$ from view location P, $\mathcal{S}$, are computed. Note here that $V = V(u) = C(u) - P$. In Figure 6 (b), these rays are extended to further pierce $C(u)$. We now have segments

of C, each of which share *homogeneous visibility*, and by shooting a ray from P toward the middle of each such curve segment, its visibility can be determined. It should be noted we only care about visible vs. invisible segments while the level of invisibility is of no interest in this application. More on this will be found in [13].

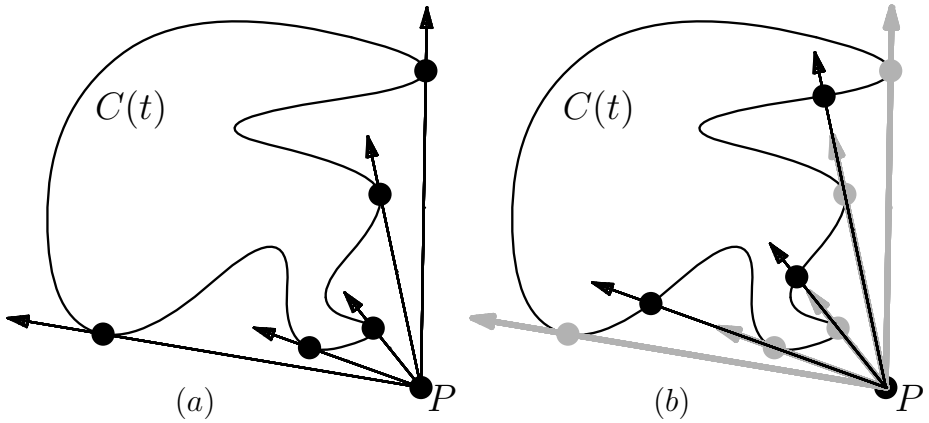

Fig. 6. A decomposition of a curve into curve segments with homogeneous visibility. In (a), the silhouette locations, $\mathcal{S}$, are computed. In (b), the silhouette rays are extended to find the locations that become visible behind $\mathcal{S}$.

Being able to determine the exact domain of $C(u)$ that is visible from V, one can create an *atlas of views* for a parameterized view location and/or direction. Several options could be considered to parameterize the view location/direction, following [13]:

- Use the unit circle $\mathcal{C}(\alpha)$ as a parameterization for all possible view directions, examining the geometry from infinity. Here, the visibility atlas will be a bivariate function, $V_h(\alpha, u)$.
- Use $C(v)$ as the view position's parameterization. Looking only into the interior of the curve, we are faced with the art gallery [3] problem. Looking from the inside out, we are examining, for example, the out-of-town coverage that guards on the perimeter of the town could provide. Here again, the visibility atlas is a bivariate function, $V_h(v, u)$, and this time it is also symmetric.
- Use an independent bivariate mapping $R(x, y)$ for the plane, possibly for the entire $\mathbb{R}^2$, to search for optimal placement of guards to watch curve $C(u)$, creating a visibility atlas of the form of $V_h(x, y, u)$. This map could be restricted to the interior of $C(u)$, thereby allowing the guards to be everywhere inside the gallery.

The visibility atlas answers the question of what is visible from a certain view position and/or direction. Seeking the minimal number of guards to watch a gallery or the minimal number of pieces of which a mold must be made to

injection-mold the part, could be answered by discretizing the problem and reducing it to a set-covering problem [5], a problem that is NP-complete [5, p. 974] in the general case.

Discretize the visibility map by sampling V_h at n different locations. If for each sampled view location/direction, only one connected interval of C is visible, the solution of the set-covering problem could be reduced to polynomial complexity [13]. By sorting all the intervals along the real line and using a greedy approach to advance along the real line with the largest interval at every step, the optimum is reached. Hence, only $O(n \log n)$ is required in such a case.

As a result, for problems where each view direction/location could hold or need hold a single interval sub-domain of C, the optimal discrete solution is tractable. This includes mold decomposition or the detection of the minimal set of parts of which a mold must be made to injection-mold a part, if possible. This is due to the fact that two disjoint intervals should be considered two different parts of the designed mold.

Figure 7 presents two examples of the mold-accessibility polynomial solution for a planar curve using the visibility atlas. In Figure 7 (a) three views are found sufficient, decomposing this curve into a three-piece mold. In Figure 7 (b), the shape must be decomposed into five pieces due to the cavities that are formed. Interestingly enough, and due to the cavities, this decomposition is made into five views that are not radially-monotone. This non-monotonicity makes the mold design a bit more complex, yet still feasible, as is shown in Figure 8. By extracting mold piece 1 in Figure 8, mold pieces 2 and 3 could be extracted as well.

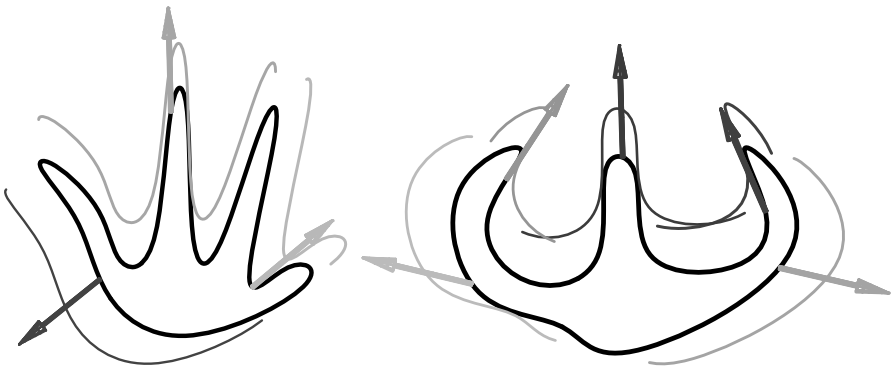

(a) (b)

Fig. 7. Two planar curves decomposed into a three-piece mold (a) and five-piece mold (b). Note the decomposition in (b) is into non-radially monotone directions (see also Figures 8 and 9).

Figure 9 presents the visibility atlases of the two curves in Figure 7 along with the three and five view directions selected to complete the coverage. Only one interval is used in each view and that interval is marked by a solid line in

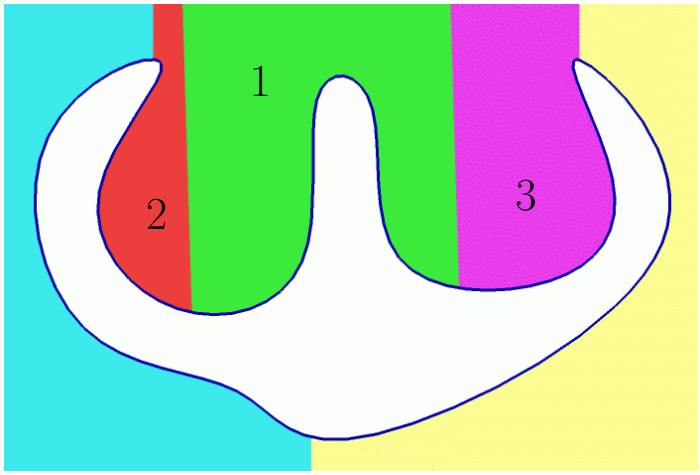

Fig. 8. The decomposition from Figure 7 yields non radially-monotone decomposition directions to form the pieces of the model. Nonetheless, a mold could be designed to realize the geometry, as is shown here.

Figure 9 whereas the other intervals in that view are marked by dotted lines. 180 sampled views were used in Figure 9 (a) while 360 sampled views were used in Figure 9 (b). While the discrete sampling is not necessarily optimal, it is conservative in the sense that the offered solutions do cover the entire domain.

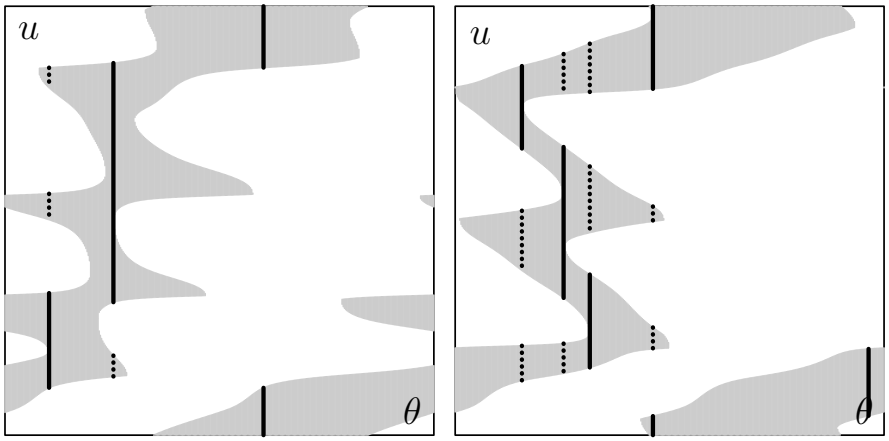

(a) (b)

Fig. 9. The visibility atlases of the curves in Figure 7. The atlas is defined as the visible u domain (in light-gray) of $C(u)$ as a function of the view direction $\theta \in [0, 360^o]$. In (a), three views are sufficient to cover the domain while in (b) five are necessary. Only the solid intervals are considered in the coverage; the dotted intervals are ignored. Note the maps are periodic and so continuous intervals could cross boundaries.

To conclude this discussion, in Figure 10, we present one example of the art gallery problem, solving for a univariate parameterization of the view location along the curve itself, $C(u)$, and looking only into the interior domain of the curve. Three guards are found sufficient in this case, as is shown in Figure 10 (a), using the symmetric visibility atlas shown in Figure 10 (b). This set-covering case is general and hence its solution has an exponential complexity in the number of guards. Again, more on this visibility problem in the context of freeform curves, including the reduction of the freeform continuous art gallery problem into a discrete set-covering problem, can be found in [13].

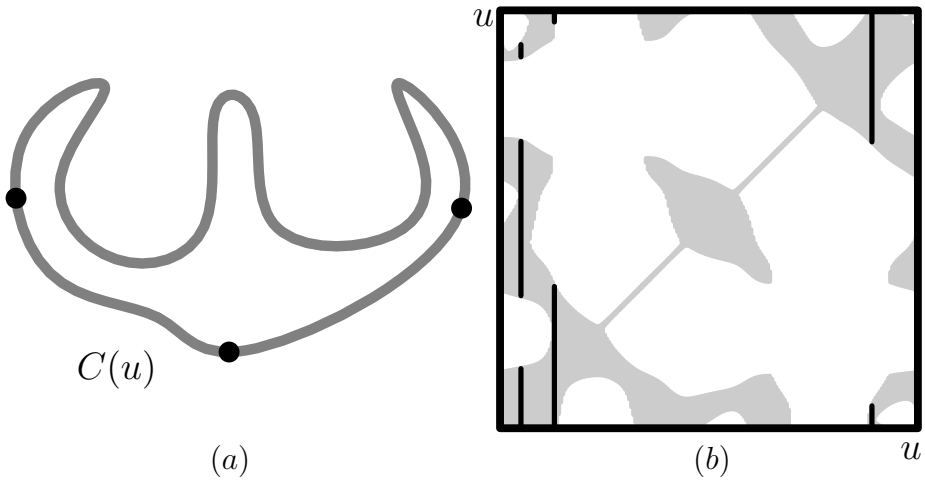

Fig. 10. Art gallery solution for the freeform shape in (a). Three guards are shown to be sufficient to cover the entire domain of this shape (as defined by the walls). In (b), the (symmetric) visibility atlas of this shape is presented along with the three selected locations whose union covers the entire parametric domain of the shape.

4 Simple Projection of Space Curves

Consider the following simple problem: Given a simple 3-space regular parametric curve $C(u)$, find all the orthographic projection directions, if they exist, along which the image of the planar projection, $C_p(u)$, is simple or self-intersection-free. Clearly, a 3-space curve could self-intersect. Yet, a self-intersection-free 3-space curve could still intersect, once projected onto some plane. Here, we seek to find (all) directions from which $C(u)$'s projection is simple.

While this problem might seem non trivial, a simple observation could clarify the solution process. Consider some viewing direction V. If there exists two different locations on C, $C(u)$ and $C(v)$, $u \neq v$, such that $(C(u) - C(v)) \times V = 0$, V cannot serve a direction that yields a simple curve projection. In other

words, we seek the directions such that for all u and v in the domain, $u \neq v$, $(C(u) - C(v)) \times V \neq 0$.

Definition 4. *The* Difference Function $\mathcal{F}_{\mathcal{M}}(u, v)$ *of a* C^1 *regular 3-space parametric curve* $C(u) : \mathcal{D} \in \mathbb{R} \rightarrow \mathbb{R}^3$ *is defined as*

$$\mathcal{F}_{\mathcal{M}}(u, v) = C(u) - C(v) : [\mathcal{D} \times \mathcal{D}] \rightarrow \mathbb{R}^3.$$

This difference map was used in the past [8, 10] to compute the distance between two different planar curves and also to find their intersection locations. The square of $||C_1(u) - C_2(v)||$ is a rational scalar field, for rationals C_i. Hence, its zeros locate the intersection locations, if any. Let $\tilde{N}_1(u)$ be an (unnormalized) normal field of planar curve $C_1(u)$ computed by rotating $C'(u)$ 90 degrees in the clockwise direction, in the plane. In [11], the scalar bivariate field of $\left\langle C_1(u) - C_2(v), \tilde{N}_1(u) \right\rangle$ for planar curves C_i was considered. Given two Bézier or B-spline planar regular curves, the control coefficients of the B-spline field of $\left\langle C_1(u) - C_2(v), \tilde{N}_1(u) \right\rangle$ is derived. Then, if all coefficients are of the same sign, the curves do not intersect. The symmetric test could be applied using $\tilde{N}_2(v)$ as $\left\langle C_1(u) - C_2(v), \tilde{N}_2(v) \right\rangle$, to provide an even better bound for intersection-free cases.

However, and going back to 3-space curves, $C(u) - C(v)$, $u \neq v$ also hints at directions that pierce the curve more than once and hence are invalid as simple curve projection directions. Centrally map all these directions of $\mathcal{F}_{\mathcal{M}}$ onto the unit sphere S^2. Every region of S^2 that is not covered by $\mathcal{F}_{\mathcal{M}}$'s central projection could then serve as a valid projection. In fact, it is sufficient to project only half of $\mathcal{F}_{\mathcal{M}}$ due to its inherent symmetry, and consequently, one should only consider the sub domain of $\mathcal{D} \times \mathcal{D}$ for which $u > v$.

Along the diagonal, $u = v$, the magnitude of $\mathcal{F}_{\mathcal{M}}$ vanishes identically. Interestingly enough, the neighborhood of the diagonal of $\mathcal{F}_{\mathcal{M}}$ represents the limit of $C(u) - C(v)$ where u and v approach the same value. In other words, the diagonal expresses the derivative of C and hence could be derived as the tangent field of C. Indeed, the tangent field, when mapped onto S^2, delineates the valid views from views where the curves starts to self-intersect. Nonetheless, the tangent field by itself is insufficient and one must consider all possible views in $C(u) - C(v)$, as will be shortly demonstrated.

A practical algorithm to detect all valid projection directions would perform the following steps:

1. Given $C(u)$, define the lifted $\mathcal{F}_{\mathcal{M}}(u, v)$ bivariate function.
2. Centrally project the sub domain of $\mathcal{F}_{\mathcal{M}}(u, v)$ for which $u > v$ onto the unit sphere S^2. This projection could, in practice, be implemented using the projection of an arbitrarily close tessellated approximation of $\mathcal{F}_{\mathcal{M}}(u, v)$.
3. Having a binary map on the unit sphere of covered vs. uncovered regions, one can either:
   (a) Extract all the uncovered regions over S^2 that contain the views with a simple projection, if any, or

(b) Find a projection direction in the middle of the uncovered regions. These centered locations offer robust projection directions that yield a simple curve projection, even after small perturbations.

Stage 3b in this proposed algorithm could be accomplished by resorting to image processing techniques. Centrally project the binary map over S^2 onto the six faces of a bounding cube. By applying image dilation procedures on all six faces, one can find the valid viewing directions, if any, that are as far as possible from the covered regions. See, for example, [12] for more on such a dilation process, in a similar context.

Figure 11 shows one example where a simple periodic 3-space C^2 cubic B-spline curve with 11 control points is projected twice, once with an intersection (in Figure 11 (a)) and once as a simple projection (in Figure 11 (b)). In each case, the projected curve is plotted on the left side and the unit sphere of directions is shown on the right, with the invalid regions painted in solid green. Also shown, in yellow, is the normalized tangent field of the curve, which is on S^2. This tangent field serves to delineate some portions of the green solid regions (the projection of $\mathcal{F}_{\mathcal{M}}$ onto S^2) but not all. The reason is that in some cases two independent regions of the curve, which are approaching, become tangent, and then intersect in the projection plane. Here the tangent field is irrelevant, yet (global) self-intersection still occurs.

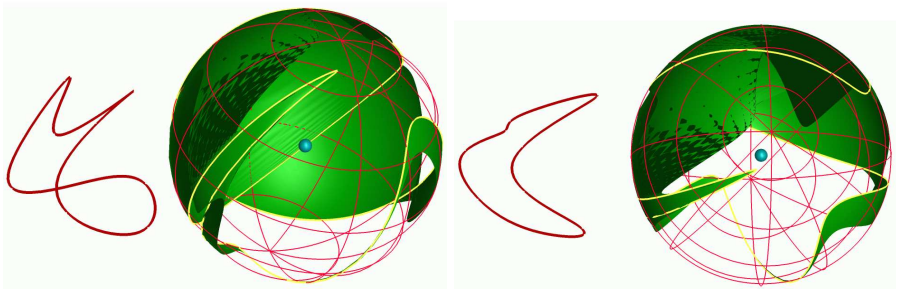

(a) (b)

Fig. 11. Computation of directions of a simple 3-space curve that yields a simple projected curve. In (a) an invalid direction is presented where the S^2 covers that direction whereas in (b) a valid direction is shown with an uncovered direction in S^2. The projection of $\mathcal{F}_{\mathcal{M}}$ onto S^2 is shown in green; the unit tangent field of the curve is shown in yellow.

Figure 12 shows a second, more complex example of a simple periodic 3-space C^2 cubic B-spline curve with 22 control points that is examined for simple projection directions. Here, the set of valid projections is narrow and yet easily identified once $\mathcal{F}_{\mathcal{M}}(u, v)$, $u > v$ is projected onto S^2. Again, appearing in yellow, the unit tangent field of the curve is also presented.

Finally, it should be noted that if $C(u_0) - C(v_0)$ is an invalid direction, so is $C(v_0) - C(u_0)$. In other words, when projecting the $\mathcal{F}_{\mathcal{M}}(u, v)$, $u > v$ field

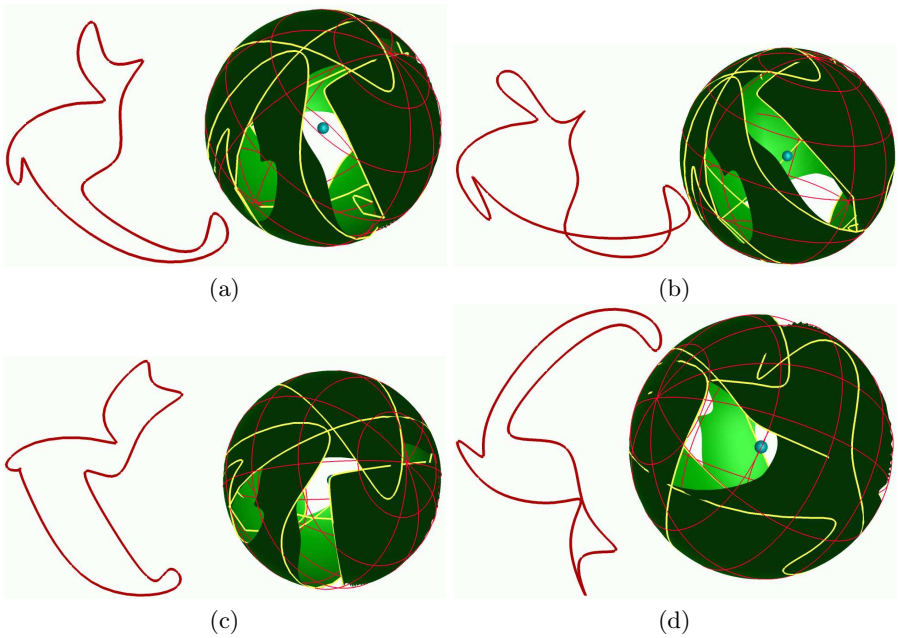

Fig. 12. Computation of the directions that yield a simple projection of a simple 3-space curve. (a) and (c) provide two valid directions whereas (b) shows an invalid one. (c) and (d) present the limiting cases of a cusp (c) and a tangency (d). The projection of $\mathcal{F}_{\mathcal{M}}$ onto S^2 is shown in green; the unit tangent field of the curve is shown in yellow.

onto S^2, the antipodal projection should be considered as well. In Figures 11 and 12, only the original projection is considered for clarity, while the center of the unit sphere is drawn as a small sphere, in cyan. The dual projection requirement is equivalent to finding a direction that "sees" the sphere's center over the background. In other words, in a valid view direction, the sphere center is covered by $\mathcal{F}_{\mathcal{M}}(u, v)$, $u > v$, from neither the front side nor the back side of the sphere.

5 Conclusions and Future Work

This work investigated a few lifting methods for extracting the global properties of freeform rational curves. The features of the orthogonality maps should be further investigated as well as extended into parallel and/or angular maps:

Definition 5. *The* Angular Function $\mathcal{A}_{\mathcal{F}}(u, v)$ *of a* C^1 *regular planar parametric curve* $C(u) : \mathcal{D} \in \mathbb{R} \rightarrow \mathbb{R}^2$ *is defined as*

$$\mathcal{A}_{\mathcal{F}}(u, v) = \frac{\langle C'(u), C'(v) \rangle^2}{\langle C'(u), C'(u) \rangle \langle C'(v), C'(v) \rangle} : [\mathcal{D} \times \mathcal{D}] \rightarrow \mathbb{R}.$$

and

Definition 6. *The* γ Angular Map $\mathcal{A}_{\mathcal{M}}[\gamma]$ *of a* C^1 *regular planar parametric curve* $C(u)$*, denoted* $\mathcal{A}_{\mathcal{M}}[C, \gamma]$*, is the constant set of the angular function,* $\mathcal{A}_{\mathcal{F}}(u, v) = \cos^2(\gamma)$*.*

Parallel and orthogonal maps are two extreme cases of angular maps, for which $\gamma = 0$ and $\gamma = \pi/2$. Being more general, the angular map lifting scheme deserves some more research. Figure 13 presents a few examples of angular maps of the curve shown in Figure 1. In (a), a parallel map ($\mathcal{A}_{\mathcal{M}}[\gamma]$ for $\gamma = 0$) is presented. The diagonal line of $u = v$ is clearly a valid solution for the parallel map. Yet, one interesting property of the parallel map, which is simple to verify, is that the number of off-diagonal branches that intersect the main diagonal exactly equal the number of inflection points in the curve, two in this case. The angular maps, for general angles, offer, for each curve location, information regarding how far one can move before the curve turns γ degrees. This information is etched onto these maps as the vertical (or horizontal) distance from the diagonal location. Figures 13 (b) and (c) show two maps of the curve in Figure 1, for γ of 30 and 60 degrees, respectively. If these maps are rebuilt using arc-length parameterizations, then they will be able to answer questions such as maximum and/or minimal turning angles of the curve per unit-length.

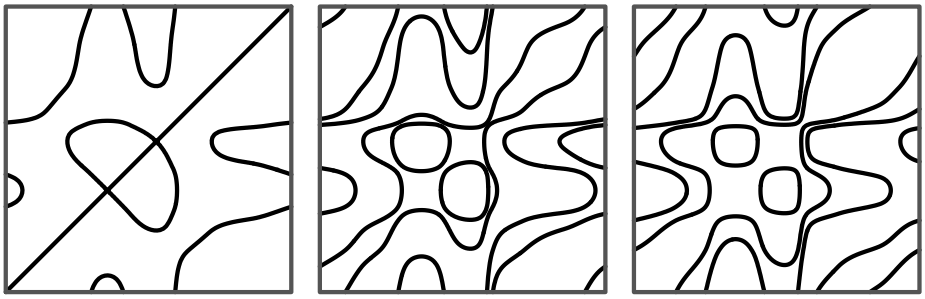

(a) $\mathcal{A}_{\mathcal{M}}[\gamma = 0]$ (b) $\mathcal{A}_{\mathcal{M}}[\gamma = 30^o]$ (c) $\mathcal{A}_{\mathcal{M}}[\gamma = 60^o]$

Fig. 13. Angular maps of the curve shown in Figure 1.

Open planar curves break the periodicity of the orthogonal/parallel/angular maps and hence would require special boundary conditioning. Piecewise C^1 planar curves also deserve attention, when investigating these maps. The C^0 locations would introduce discontinuities into the angular functions and their proper handling and map extraction would be more difficult.

In Section 4, a method to derive the proper projection directions of a simple space curve that would yield a simple curve has been proposed. This method could clearly be used to find directions from which surface $S(u, v)$ is completely visible. When the 4-variate vector field of $F(u, v, s, t) = S(u, v) - S(s, t)$ is projected onto S^2, its uncovered regions would yield the completely visible projection directions, if any. It should be noted that this computation is not the same

as finding a direction that presents no silhouettes. A surface could possess no silhouettes from a certain view direction and yet still occlude itself.

References

1. H.-K. Ahn, M. de Berg, P. Bose, S. Cheng, D. Halperin, J. Matoušek, and O. Cheong. Separating an object from its cast, Computer-Aided Design, Vol 34, pp 547–559, 2002.
2. A. Appel. The notion of quantitative invisibility and the machine rendering of solids, Proc. ACM National Conference, Washington, DC, 387–393, 1967.
3. M. de Berg, M. van Kreveld, M. Overmars, O. Schwarzkopf. Computational Geometry, Algorithms, and Applications (2nd ed.), Springer-Verlag, Berlin, 2000.
4. M. Bloomenthal. Approximation of sweep surfaces by tensor product B-splines, Tech Reports UUCS-88-008, University of Utah, 1988.
5. T. H. Cormen, C. E. Leiserson, and R. L. Rivest. Introduction to Algorithms, MIT Press and McGraw-Hill, 1990.
6. M. do Carmo. Differential Geometry of Curves and Surfaces. Prentice Hall, 1976.
7. G. Elber and E. Cohen. Hidden curve removal for free form surfaces, Computer Graphics (Proc. SIGGRAPH), 24 (1990), 95–104.
8. G. Elber. Symbolic and numeric computation in curve interrogation, Computer Graphics Forum, Vol 14 pp 25–34, 1995.
9. G. Elber. Multiresolution curve editing with linear constraints, The Journal of Computing & Information Science in Engineering, Vol 1, No 4, pp 347–355, Dec 2001.
10. G. Elber. Trimming local and global self-intersections in offset curves using distance maps, Proc. of the 10th IMA Conference on the Mathematics of Surfaces, Leeds, UK, pp 213–222, September 2003.
11. G. Elber. Distance separation measures between parametric curves and surfaces toward intersection and collision detection applications, Proceedings of COMPASS 2003, Schloss Weinberg, Austria, October 2003.
12. G. Elber, X. Chen, and E. Cohen. Mold accessibility via Gauss map analysis, Shape Modeling International 2004, Genova, Italy, pp 263–274, June 2004.
13. G. Elber, R. Sayegh, G. Barequet, and R. R. Martin. Two-dimensional visibility charts for continuous curves, to Appear in Shape Modeling International 2005, Boston, USA, June 2005.
14. C. Gonzales-Ochoa, S. Mccamnon, and J. Peters. Computing moments of objects enclosed by piecewise polynomial surfaces, ACM Transactions on Graphics, Vol 17, No 3, pp 143–157, July 1998.
15. S. Hahmann, G.-P. Bonneau, and B. Sauvage. Area preserving deformation of multiresolution curves, submitted.
16. J. Keyser, T. Culver, D. Manocha and S. Krishnan, Efficient and exact manipulation of algebraic points and curves, Computer-Aided Design, Vol 32, No 11, pp 649–662, Sep 2000.
17. F. Klok. Two moving coordinate frames for sweeping along a 3D trajectory, Computer Aided Geometric Design, Vol 3, No 3, pp 217–229, 1986.
18. A. Rappaport, A. Sheffer, and M. Bercovier. Volume-preserving free-form solids, IEEE Transactions on Visualization and Computer Graphics, Vol 2, No 1, pp 19–27, March 1996.
19. T. Woo. Visibility maps and spherical algorithms, Computer-Aided Design, 26 (1994), pp 6–16.